Impact of a New Sea Ice Thermodynamic Formulation in the CESM2 sea ice component

David A. Bailey[1], Marika M. Holland[1], Alice K DuVivier[1], Elizabeth C. Hunke[2], Adrian K. Turner[2]

[1]National Center for Atmospheric Research, Boulder, CO

[2] Los Alamos National Laboratory, Los Alamos, NM

Abstract

The sea ice component of the Community Earth System Model version 2 (CESM2) contains new "mushy-layer" physics that simulates prognostic salinity in the sea ice, with consequent modifications to sea ice thermodynamics and the treatment of melt ponds. The changes to the sea ice model and their influence on coupled model simulations are described here. Two simulations were performed to assess the changes in the vertical thermodynamics formulation with prognostic salinity compared to a constant salinity profile. Inclusion of the mushy layer thermodynamics of Turner et al. (2013) in a fully coupled earth system model produces thicker and more extensive sea ice in the Arctic, with relatively unchanged sea ice in the Antarctic compared to simulations using a constant salinity profile. While this is consistent with the findings of uncoupled ice-ocean model studies, the role of the frazil and congelation growth is more important in fully coupled simulations. Melt pond drainage is also an important contribution to simulated ice thickness differences as also found in the uncoupled simulations of Turner and Hunke 2015. The changes in thermodynamics and resulting ice state modifies ice-ocean-atmosphere fluxes with impacts on the atmosphere and ocean states, particularly temperature.

1. Introduction

Sea ice in the real world is a combination of solid ice and salty brine trapped within the ice. The size of brine pockets and their consequent salinity and temperature can vary to maintain thermal equilibrium with the surrounding ice (Schwerdtfeger, 1963). The net salinity content of the sea ice can also change over time due to various processes such as gravity drainage and meltwater flushing (e.g. Weeks and Ackley, 1986). The resulting sea ice salinity affects the thermal properties of the ice, including its heat capacity and the heat required for melting. The ice salinity and consequent porosity also affect the flow of nutrients within sea ice with impacts on sea ice biogeochemistry (Elliott et al. 2017) and can modify the strength of the ice (Turner et al. 2013).

The influence of ice salinity on sea ice thermodynamics has been considered in modeling of the ice cover in climate simulations for quite some time (e.g. Maykut and Untersteiner, 1971; Semtner, 1976; Bitz and Lipscomb, 1999). However, traditionally this has used a prescribed and non-varying salinity profile based on observations. Considerable previous work has assessed processes driving sea ice salinity variations, primarily in one-dimensional sea ice models. This includes work on how gravity drainage (e.g. Cox and Weeks, 1988; Notz and Worster, 2009; Turner et al., 2013; Griewank and Notz, 2013, Rees Jones and Worster, 2014), and melt water flushing (e.g. Vancoppenolle et al., 2007; Jeffrey et al., 2011) affect the sea ice salinity structure.

Several recent efforts have incorporated prognostic salinity into large-scale sea ice models. Vancoppenolle et al. (2009) simulated a variable, vertically-averaged salinity within the Louvain-la-Neuve sea ice model (LIM3) and tested its use in global ice-ocean coupled simulations. While the total salinity can vary in this implementation, the vertical distribution is prescribed. More recently, Turner et al. 2013 introduced a “mushy-layer” thermodynamic scheme (hereafter

MUSHY) for large-scale sea ice models. In this formulation, the vertical salinity profile in the sea ice is prognostic and the sea ice is formed as a mass of solid ice and salty brine. Turner and Hunke (2015) comprehensively evaluated the change from Bitz and Lipscomb, 1999 (hereafter BL99) thermodynamics, which has a prescribed vertical salinity profile, to MUSHY within the standalone Los Alamos Sea Ice Model CICE (Hunke et al., 2015) in global simulations with prescribed atmospheric and oceanic forcing, performing pairs of experiments in which the only difference was the physics change being tested. In these runs, the atmosphere and ocean were not able to change in response to changes in the sea ice. Their runs produced thicker and more extensive sea ice in the Arctic with MUSHY, while in the Antarctic there was similar sea ice with MUSHY and BL99. The primary reason behind the northern hemisphere differences in their simulations was due to the modification of melt pond characteristics with the parameterization of melt pond drainage in the MUSHY configuration. Secondary factors were the shortwave formulation near the melt point within the ice and differences in how ice grows and melts between the formulations. In the southern hemisphere they found that snow-ice formation was more important but did not contribute to significant differences in the sea ice volume and area.

The Community Earth System Model version 2 (CESM2; Danabasoglu et al. 2020) is one of the first Coupled Model Intercomparison Project phase 6 (CMIP6) models to move to this newer thermodynamic formulation. CESM2 contains version 5.1.2 of the Los Alamos Sea Ice Model (CICE; Hunke et al. 2015) and includes support for the Sea Ice Model Intercomparison Project (SIMIP) variable request (Notz et al. 2016). This version of CICE features a number of new physics options including the MUSHY thermodynamics of Turner et al. (2013) and the level-ice melt pond scheme of Hunke et al. (2013). The main change with the new MUSHY physics of Turner et al.

2013 is the inclusion of the variable, prognostic salinity profile. In the BL99 thermodynamic formulation used in CESM1, a fixed prescribed salinity profile based on observations was applied.

This manuscript is focused on understanding the influence of the new sea ice thermodynamic formulation within the coupled context of CESM2. As discussed in section 2, this involves comparing fully coupled simulations with MUSHY to simulations which use BL99. An assessment of the sea ice mean state and mass budget differences between the simulations in both hemispheres is provided and the influence on coupled simulation characteristics is discussed. Comparison of CESM2 sea ice mass budgets with other models contributed to CMIP6 are analyzed in Blockley et al. (2020) and a number of characteristics of the sea ice as simulated in CESM2 runs are documented in DuVivier et al. (2020, submitted), Singh et al. (2020, submitted) and DeRepentigny et al. (2020, submitted).

2. Model and Experiment Description

As described by Hunke et al. (2013), the CICE model used here is a dynamic-thermodynamic model which incorporates an ice thickness distribution. Sea ice dynamics is simulated using an elastic-viscous-plastic rheology (Hunke and Dukowicz, 2002) with a linear remapping advection scheme (Lipscomb and Hunke, 2004). The ice thickness distribution is resolved with five ice thickness categories and a single open water category.

A new aspect of the CICE model used here is the inclusion of prognostic sea ice salinity and associated changes in the ice thermodynamics. Turner and Hunke (2015) fully describe this MUSHY thermodynamic formulation and here we highlight the primary details. The model

93 simulates a time-varying and vertically-resolved prognostic salinity and its influence on
94 thermodynamic properties of the sea ice. The migration of water and brine through the ice is
95 handled through drainage and flushing processes, allowing the bulk salinity to change over time.
96 This is in contrast to the BL99 scheme which has a prescribed salinity profile. In both formulations,
97 the ice salinity impacts thermodynamic characteristics and the internal ice energy is a function of
98 the salt content.
99
100 With the prognostic salinity profile there are several associated differences including the freezing
101 point calculation, the thermal conductivity in the sea ice, the growth of sea ice including frazil ice
102 formation, snow-ice formation, gravity drainage and melt pond flushing (Turner et al. 2013). Also,
103 for consistency with the Turner et al. (2013) thermodynamics, the salinity dependent freezing point
104 of Assur 1958 was used for both the sea ice and ocean components at the sea ice-ocean interface.
105 The melt pond formulation of Hunke et al. (2013) considers the fraction of level ice (as a tracer)
106 versus deformed ice, which directly impacts the melt pond concentration and depth. In addition to
107 the new physics, the vertical levels in CESM2 were increased from 4 to 8 in the sea ice and from
108 1 to 3 in the snow, in order to better resolve the temperature and salinity gradients in the sea ice.
109
110 The sea ice mass budget terms are also impacted by the MUSHY formulation in that sea ice forms
111 a mass of solid ice and salty brine. This directly impacts the fluxes of water and heat between the
112 sea ice and ocean. The salt flux is influenced by the mass of water exchange, but a salinity of 4
113 psu is still assumed here as in BL99 for simplicity of coupling with the ocean model. Snow ice
114 formation occurs when the weight of the snow pushes the snow-ice interface below the waterline.
115 In this process, the MUSHY scheme explicitly accounts for seawater flooding of the snow pack,

thereby affecting the mass of snow-ice formed, whereas in BL99 the snow is just compressed into ice with no addition of seawater. Melt pond properties are also influenced by the MUSHY formulation as it allows for melt ponds to drain based on the sea ice porosity, calculated with the prognostic salinity and through parameterized macroscopic holes. On the other hand, the BL99 scheme only allows drainage due to the salinity-based ice porosity.

To diagnose the influence of the new sea ice physics on CESM2, two complementary, preindustrial model experiments were performed: the first with the MUSHY thermodynamics of Turner et al. (2013) and the second with the BL99 thermodynamics of Bitz and Lipscomb (1999). In the fully-coupled CESM2 experiments presented here, the only difference between the simulations is the value of the CICE parameter "ktherm," which selects the vertical thermodynamics scheme. These simulations were both branched from the CESM2 CMIP6 pre-industrial control run (Danabasoglu et al. 2020) at year 880 and each ran for 50 years. The simulations shown here used only the single-layer snow formulation, but the results were not significantly different from the three-layer simulations (not shown). Additionally, in the CESM2 version of CICE5, we have added a shortwave adjustment for both thermodynamics schemes to overcome a coupled instability that can cause internal sea ice layers to melt completely in a single timestep, generating very large fluxes of fresh water. By rerouting excess shortwave (when the internal temperature is very close to melting) from inside the sea ice to the top melt, this change allows the sea ice to melt more gradually. This shortwave adjustment is included in both our MUSHY and BL99 simulations.

3. Results

3.1. **Sea ice mean state and variability**

Sea ice thickness is significantly larger in the MUSHY configuration as shown in Figure 1a. While the southern hemisphere thickness differences are significant in some locations (Figure 1b), they are generally small. These coupled results are consistent with Turner and Hunke (2015), and the processes/causes leading to the difference will be expanded upon in the next section. Similarly, the annual mean sea ice concentration (Figure 2) is significantly higher in the MUSHY run in both the Arctic and Antarctic, though the difference is smaller in the Antarctic. As with the sea ice thickness, the mean Arctic snow depth is larger in the MUSHY run (Figure 3). This is mostly due to the larger autumn ice area which provides a platform for snow to accumulate. As discussed later, differing snow melt in the simulations also plays a role in the seasonal evolution of the albedo.

Considering the annual cycle of ice conditions, we find that the northern hemisphere sea ice is significantly more extensive in the MUSHY simulation in all months (Figure 4a). Although it is useful to put these results in the context of the observations, it is worth noting that the NSIDC climatology shown here (Fetterer et al. 2017) is for present day conditions, while these simulations are pre-industrial. Therefore, a direct match between the model and observations should not be expected. More extensive sea ice is consistent with the thicker ice in the MUSHY experiments and the strong coupling between ice thickness and ice area during summer months. In the southern hemisphere (Figure 4b), the sea ice extent in the two simulations is statistically indistinguishable in all months.

Notably, the northern hemisphere differences originate almost immediately in the simulations, and the annual mean Arctic sea ice volumes (Figure 5a) and ice area (Figure 5c) are significantly larger in the MUSHY run throughout the entire 50 year experiments. In the southern hemisphere, the

volume and area are significantly different (Figures 5b and d), but the differences are much smaller than in the northern hemisphere. The 50-year sea ice volume mean (Table 1) are all significant to the 5% level in both hemispheres based on a t-test. The 50-year variances (Table 1) are not significantly different in either hemisphere based on an F-test. That is, the MUSHY simulation is thicker and more extensive overall in both hemispheres, but the variability is unchanged. However, although these 50-year simulations are designed to account for interannual variability, they may not capture the full extent of decadal variability.

3.2. Mass budgets

To address the question of why the MUSHY simulation has thicker ice, we examine the mass budget in our two simulations using the SIMIP (Notz et al. 2016) variables. Figure 6 shows the overall sea ice mass budget components along with differences (MUSHY minus BL99) of the mass budget terms. Sea ice mass budget differences can arise from both the different thermodynamic treatment in the simulations and changes in the mean state.

In the net (black) Arctic seasonal mass budget (Figure 6a), the BL99 case (solid lines) has a slightly larger amplitude annual cycle as a result of more growth in winter and more melt in summer. The larger summer melt is the result of greater top and bottom melt in the BL99 scheme. The enhanced BL99 growth in winter is largely due to enhanced congelation growth (cyan). This is consistent with the thinner ice and snow in BL99, which allows for more conduction of heat from the ice-ocean interface. The MUSHY scheme has larger frazil ice growth (magenta) in winter, but it is not sufficiently large to lead to more total winter growth. The increased frazil formation is expected because of the way the MUSHY physics functions, forming ice as a combination of solid and

liquid sea water. The liquid is trapped within the sea ice and hence the net thickness of sea ice and water together is thicker (Turner et al. 2013). It is also interesting to look at differences in the mass budget where both simulations have at least 15% concentration in Figure 6c. Here we see that the congelation and frazil differences are both much smaller between the two schemes. Since regions with concentration less than 15% would be dominated by frazil growth and enhanced congelation growth, it makes sense that when we only look at places where both experiments have sea ice concentration above 15% the differences in these growth terms become smaller.

The snow mass budget on the surface of the sea ice (Figure 7) exhibits a slight shift in the seasonal cycle; BL99 has larger snow melt in the early summer, while MUSHY has larger snow melt late in the summer. In areas where both simulations have at least 15% concentration (Figure 7c), the main factor in the seasonal snow mass cycle difference is the snow melt. The factors in the snow seasonal cycle will be discussed in the next section.

In the Antarctic (Figure 8), the net mass budget is similar for the two thermodynamic formulations, but the individual mass budget terms contributing to this are different in BL99 and MUSHY. MUSHY has significantly more frazil growth and snow-ice formation than BL99. This is largely compensated for by decreased congelation growth relative to BL99. There is little difference in top melt, but considerably stronger bottom melt in the MUSHY simulation. The bottom melt in the Southern Hemisphere is stronger in the MUSHY case because the sea ice is saltier than the BL99 sea ice (not shown) and hence begins to melt at a lower temperature, so it is easier to melt overall. The difference in mass budget terms, particularly the frazil ice, appears to play a role in the thinner and less extensive Antarctic sea ice in CESM2 compared to CESM1 (Singh et al. 2020).

208 There are regional differences in the SH sea ice mass budget where frazil ice is more important
209 near the coast and snow-ice formation is more important in the open pack (not shown).
210
211 **3.3. Arctic Melt ponds and surface albedos**
212 It appears that the decreased Arctic melt (less negative) in MUSHY is a consequence of the sea
213 ice physics, whereas the decreased growth (less positive) is associated with the thicker and more
214 insulating mean sea ice state. To assess why Arctic surface melt is different between the
215 formulations, we examine the annual cycle of snow fraction, melt pond fraction and broadband
216 albedo (Figure 9). The snow fraction (Figure 9a) is higher in the MUSHY scheme, and the
217 radiatively active pond coverage (that is, the fraction of liquid water not hidden by snow, used in
218 the shortwave radiation computation, Figure 9b) is smaller. The MUSHY scheme allows for more
219 porous ice (macroscopic drainage) through which melt ponds drain, thus reducing the overall melt
220 pond coverage. The combination of reduced melt pond fraction and higher snow fraction leads to
221 a higher broadband albedo in mid-summer for MUSHY (Figure 9c). In the fall, the melt pond
222 fraction is greater in the MUSHY scheme, but the resulting lower albedo occurs when sunlight is
223 disappearing rapidly and as a result is not as important for the surface energy balance.
224
225 Maps of mean spring (April-May-June) snow depth (Figure 3) and the radiatively active pond
226 fraction and level ice fraction (Figure 10) all show large differences in the central Arctic. Pond
227 coverage is a function of the snow cover, surface melt, pond drainage, and level ice fraction –
228 ponds are located only on level ice in the melt pond scheme used in both simulations. The MUSHY
229 experiment has less level ice in the central Arctic (Figure 10b), which reduces pond area coverage.
230 It is not clear why the level ice tracer is impacted by the choice of MUSHY vs. BL99

thermodynamics. A possible reason for the level ice differences is the mean sea ice state differences in the two experiments and surface melt differences. These factors lead to less pond coverage in the MUSHY experiment and hence a higher broadband albedo and less top melt of the sea ice in the central Arctic. In the southern hemisphere, because snow remains longer on the sea ice hiding liquid water, melt ponds are not a dominant factor.

3.4. Coupled Impacts

To assess the potential coupled impacts of the change in the vertical thermodynamic schemes, the Arctic surface air temperature is shown in Figure 12. The thicker ice and deeper snow in MUSHY lead to colder conditions over the ice pack. The changes in surface air temperature (Figure 12a) are significant over the central Arctic. The higher surface albedo in the MUSHY case changes the surface energy balance by reflecting more shortwave energy back to the atmosphere, which results in less surface melt and more snow cover. This change has a positive feedback on ice growth in the coupled model, because the sea ice melts less in summer, dominating the slower growth of thicker ice in the fall. This feedback is not present in a forced ice-ocean experiment, as was shown by Turner et al. (2015).

Similarly, the sea surface temperature and salinity (Figure 13) show a colder and saltier central Arctic where the MUSHY has thicker ice due to enhanced ice growth. The colder temperatures are likely due to lower freezing point temperatures. The North Atlantic is colder and fresher due to increased sea ice export from the Arctic. The differences in the ocean fields are somewhat muted as these were only 50-year simulations and there would likely have a been a stronger response in longer, better ocean-equilibrated simulations.

4. Discussion and Conclusions

CESM2 (Danabasoglu et al., 2020) incorporates a new sea ice model component that includes prognostic salinity and treats sea ice as a two-phase mushy layer following Turner et al. (2013). We find that the MUSHY scheme produces thicker and more extensive ice overall in both hemispheres relative to the Bitz and Lipscomb (BL99) thermodynamics used in earlier CESM versions. While this agrees with the stand-alone sea ice results of Turner and Hunke (2015), the reasons for it differ, partly due to coupled interactions with the atmosphere and ocean. Turner and Hunke (2015) found that the difference in melt pond drainage was the leading factor for thicker ice in MUSHY, and changes in the shortwave formulation and the way thickness changes are computed (i.e. the uptake of sea water and ice in the MUSHY scheme) were also found to be important. In our fully-coupled CESM2 simulations, both the MUSHY and BL99 thermodynamic schemes use the same shortwave formulation, so this radiative factor has been removed in our comparisons. While the Arctic melt pond coverage is different between the simulations, and contributes to the differences in top melt, differences in frazil ice and congelation ice formation also play a role. The MUSHY simulation has less surface melt and more frazil ice formation, which is offset by reduced congelation growth. This balance of melt and growth leads to thicker ice in the MUSHY run. These differences are particularly important in regions with less than 15% sea ice cover, where the sea ice is both thinner and less extensive.

Draining of melt ponds and reduced surface melt are key differences for the melt pond coverage and hence the surface albedo. However, differences in undeformed or level ice also play a role in the melt pond coverage. Melt ponds also feed back into the snow seasonal cycle; the thicker ice in

276 the MUSHY simulations allows for more snow accumulation and hence less radiatively active
277 ponds.
278
279 In the southern hemisphere, sea ice has much less top melt and snow-ice formation plays a much
280 larger role in these experiments. While individual mass budget terms differ in the MUSHY
281 simulation relative to BL99, the net budget is similar, and the mean sea ice state differences are
282 much smaller for the Antarctic than the Arctic. Despite the balance in terms being quite similar in
283 the Antarctic sea ice, the regional differences in these terms show both positive and negative
284 differences in the thickness and area. In particular, frazil ice formation is more important near the
285 coast and snow-ice formation is more important in the open pack. Aspects of this are discussed in
286 Singh et al. (2020).
287
288 The change to the thermodynamics with the MUSHY physics does affect the sea ice thickness in
289 CESM2. However, in comparisons of CESM2 and CESM1, a number of other physics changes
290 are present across the atmosphere and ocean components. These changes also have an important
291 influence on the sea ice simulation and its feedbacks within the coupled system (DuVivier et al.
292 2020; Singh et al. 2020).
293
294 **Model and Data Availability**
295 Previous and current CESM versions are freely available at www.cesm.ucar.edu:/models/cesm2/.
296 The CESM datasets used in this study will be made available upon acceptance of the manuscript

from the Earth System Grid Federation (ESGF) at esgf-node.llnl.gov/search/cmip6, or from the NCAR Digital Asset Services Hub (DASH) at data.ucar.edu, or from the links provided from the CESM web site at www.cesm.ucar.edu.

Acknowledgments

The CESM project is supported primarily by the National Science Foundation (NSF). This material is based upon work supported by the National Center for Atmospheric Research (NCAR), which is a major facility sponsored by the NSF under Cooperative Agreement No. 1852977. Computing and data storage resources, including the Cheyenne supercomputer (doi:10.5065/D6RX99HX), were provided by the Computational and Information Systems Laboratory (CISL) at NCAR. ECH is supported through the Regional and Global Modeling and Analysis focus of the Earth System Model Dynamics program within the Department of Energy's Office of Biological and Environmental Research.

References

Assur, A. Composition of sea ice and its tensile strength. In Arctic sea ice; conference held at Easton, Maryland, February 24–27, 1958, volume 598 of Publs. Natl. Res. Coun. Wash., pages 106–138, Washington, DC, US, 1958.

Bitz, C.M. and W.H. Lipscomb, 1999: An energy-conserving thermodynamic sea ice model for climate study. J. Geophys. Res. Oceans, 104(C7):15669–15677, doi: 10.1029/1999JC900100.

Bitz, C.M., and G.H. Roe, 2004. A Mechanism for the High Rate of Sea-Ice Thinning in the Arctic Ocean. Journal of Climate, 17, 3622–31.

Cox, G. F. N., and W. F. Weeks, 1988: Numerical simulations of the profile properties of undeformed first-year sea ice during the growth season. J Geophys Res Oceans, 93(C10), 12449—12460. doi: 10.1029/JC093iC10p12449.

Danabasoglu, G., Lamarque, J. -F., Bachmeister, J., Bailey, D. A., DuVivier, A. K., Edwards, J., Emmons, L. K., Fasullo, J., Garcia, R., Gettelman, A., Hannay, C., Holland, M. M., Large, W. G., Lawrence, D. M., Lenaerts, J. T. M., Lindsay, K., Lipscomb, W. H., Mills, M. J., Neale, R., Oleson, K. W., Otto-Bliesner, B., Phillips, A. S., Sacks, W., Tilmes, S., van Kampenhout, L., Vertenstein, M., Bertini, A., Dennis, J., Deser, C., Fischer, C., Fox-Kember, B., Kay, J. E., Kinnison, D., Kushner, P. J., Long, M. C., Mickelson, S., Moore, J. K., Nienhouse, E., Polvani, L., Rasch, P. J., Strand, W. G., 2020: The Community Earth System Model version 2 (CESM2). J Adv Model Earth Sys, 12(2), doi: 10.1029/2019MS001916.

DeRepentigny, P., Jahn, A., Holland, M. M., Smith, A. (2020) Arctic Sea Ice in the Two Community Earth System Model Version 2 (CESM2) Configurations During the 20th and 21st Centuries. J Adv Model Earth Sys (Submitted).

DuVivier, A. K., M. M. Holland, J. E. Kay, S. Tilmes, A. Gettelman, D. A. Bailey, 2020: Arctic and Antarctic sea ice state in the Community Earth System Model Version 2. J. Geophys. Res. Oceans (Under Review).

Elliott, S.; Jeffery, N.; Hunke, E.; Deal, C.; Jin, M.; Wang, S.; Elliott Smith, E.; Oestreicher, S. Strategies for the Simulation of Sea Ice Organic Chemistry: Arctic Tests and Development. Geosciences 2017, 7, 52.

Fetterer, F., K. Knowles, W. N. Meier, M. Savoie, and A. K. Windnagel. 2017, updated daily. Sea Ice Index, Version 3. [1984-2015]. Boulder, Colorado USA. NSIDC: National Snow and Ice Data Center. doi: 10.7265/N5K072F8.

Griewank, P. J. and D. Notz, 2013: Insights into brine dynamics and sea ice desalination from a 1-D model study of gravity drainage. J Geophys Res Oceans, 118(7), 3370—3386. doi: 10.1002/jgrc.20247

Hunke, E. C. and J. K. Dukowicz. The Elastic-Viscous-Plastic sea ice dynamics model in general orthogonal curvilinear coordinates on a sphere—Effect of metric terms. Mon. Wea. Rev., 130:1848–1865, 2002.

Hunke, E. C., D. A. Hebert, and O. Lecomte. 2013: Level-ice melt ponds in the Los Alamos Sea Ice Model, CICE. Ocean Mod., 71:26–42.

Hunke E. C., W. H. Lipscomb, A. K. Turner, N. Jeffery, and Scott Elliott. CICE: The Los Alamos Sea Ice Model. Documentation and Software User's Manual. Version 5.1. T-3 Fluid Dynamics Group, Los Alamos National Laboratory, Tech. Rep. LA-CC-06-012, 2015.

Jahn, A, K. Sterling, M. M. Holland, J. E. Kay, J. A. Maslanik, C. M. Bitz, D. A. Bailey, J. Stroeve, E. C. Hunke, W. H. Lipscomb, D. Pollak, 2012: Late 20th century simulation of Arctic sea ice and ocean properties in CCSM. J. Climate, 25, 1431-1452. doi:10.1175/JCLI-D-11-00201.1.

355 Jeffery, N., E. C. Hunke, and S. M. Elliott, 2011: Modeling the transport of passive tracers in sea
356 ice. J Geophys Res Oceans, 116, C07020, doi: 10.1029/2010JC006527.
357 Keen, A., E. Blockley, D. A. Bailey, J. B. Debernard, M. Bushuk, D. Docquier, S. O'Farrell, D.
358 Schroeder, N. Swart, and T. Toyoda, 2019: An inter-comparison of the mass budget of the Arctic
359 sea ice in CMIP6 models. Cryosphere (Under Review).
360 Kwok, R., and G. F. Cunningham, 2008: ICESat Over Arctic Sea Ice: Estimation of Snow Depth
361 and Ice Thickness. Journal of Geophysical Research 113(C08010), doi: 10.1029/2008JC004753.
362 Lipscomb, W. H. and E. C. Hunke. Modeling sea ice transport using incremental remapping. Mon.
363 Wea. Rev., 132:1341–1354, 2004.
364 Maykut, G. A., & Untersteiner, N. (1971). Some results from a time-dependent thermodynamic
365 model of sea ice. J. Geophys Res, **76**, 1550– 1575. doi:10.1029/JC076i006p01550
366 Notz, D. and M. G. Worster, 2009: Desalination processes of sea ice revisited. J Geophys Res
367 Oceans, 114, C05006, doi: 10.1029/2008JC004885.
368 Notz, D., A. Jahn, M Holland, E. Hunke, F. Massonnet, J. Stroeve, B. Tremblay, and M.
369 Vancoppenolle, 2016: The CMIP6 Sea-Ice Model Intercomparison Project (SIMIP):
370 understanding sea ice through climate-model simulations. Geosci. Model Dev., 9, 3427–3446.
371 doi:10.5194/gmd-9-3427-2016.
372 Rees Jones, D. W. and M. G. Worster, 2014: A physically based parameterization of gravity
373 drainage for sea-ice modeling. J Geophys Res Oceans, 119(9), 5599—5621. doi:
374 10.1002/2013JC009296.
375 Singh HAS, Landrum LL, and Holland MM. "An Overview of Antarctic Sea Ice in the CESM2:
376 Analysis of the Seasonal Cycle, Predictability, and Atmosphere-Ocean-Ice Interactions."
377 Submitted to JAMES (March 2020).

Semtner, A. J. 1976: A Model for the Thermodynamic Growth of Sea Ice in Numerical Investigations of Climate. J Phys Oceanogr, 6, 379—389.

Schwerdtfeger, P., 1963: The Thermal Properties of Sea Ice. J. Glaciol. 36(4), 789-807. doi: 10.3189/S0022143000028379

Turner, A. K., E. C. Hunke, and C. M. Bitz, 2013: Two modes of sea-ice gravity drainage: A parameterization for large-scale modeling. J. Geophys. Res. Oceans, 118, 2279—2294. doi: 10.1002/jgrc.20171.

Turner, A. K., and E. C. Hunke, 2015: Impacts of a mushy-layer thermodynamic approach in global sea-ice simulations using the CICE sea-ice model. J. Geophys. Res. Oceans, 120, 1253–1275, doi:10.1002/2014JC010358.

Vancoppenolle, M., T. Fichefet, and H. Goosse, 2009: Simulating the mass balance and salinity of Arctic and Antarctic sea ice. 2. Importance of sea ice salinity variations. Ocean Modelling, 27(1-2), 54—69. doi: 10.1016/j.ocemod.2008.11.003.

Vancoppenolle, M., T. Fichefet, and C. M. Bitz, 2007: Summer landfast sea ice desalination at Point Barrow, Alaska: Modeling and observations. J Geophys Res Oceans, 112, C04022, doi: 10.1029/2006JC003493.

Weeks, W.S. and S.F. Ackley, The growth, structure and properties of sea ice, in The Geophysics of Sea Ice, NATO ASI Series, Se. B, vol 146, edited by N. Untersteiner, pp 9-164, Plenum, New York, 1986

Table 1: Annual Northern Hemisphere (NH) and Southern Hemisphere (SH) mean sea ice volume (10^{13} m^3) and area (10^{12} m^2) and interannual variance.

	BL99 Mean	BL99 Variance	MUSHY mean	MUSHY variance
NH Ice Volume	1.77	0.02	2.31	0.012
NH Ice Area	10.13	0.06	10.72	0.055
SH Ice Volume	1.45	0.01	1.53	0.01
SH Ice Area	11.00	0.12	11.35	0.14

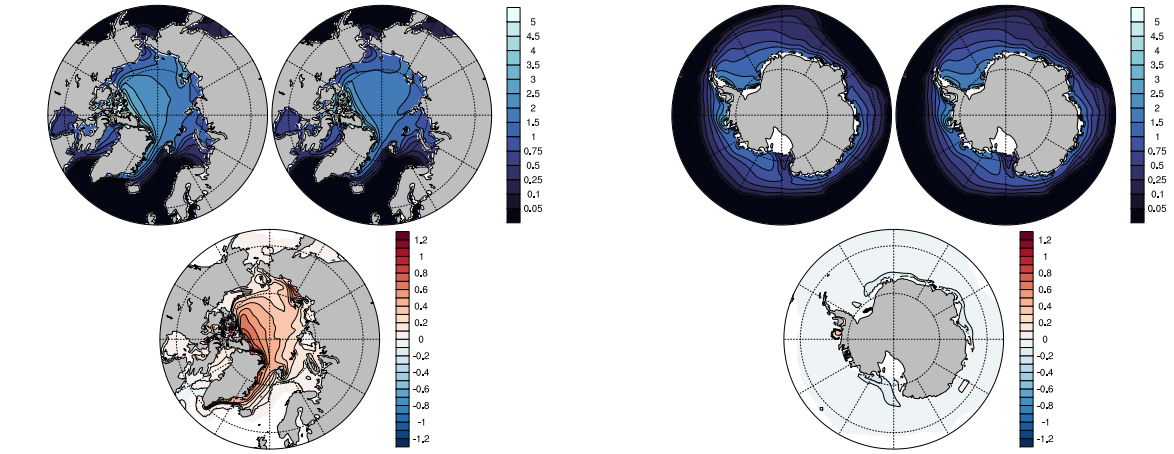

a b

Figure 1. Mean annual sea ice thickness (m) and differences for (a) NH and (b) SH. MUSHY is top left and BL99 is top right. Differences, at bottom center, show MUSHY-BL99 and are only shown where significant at the 5% level.

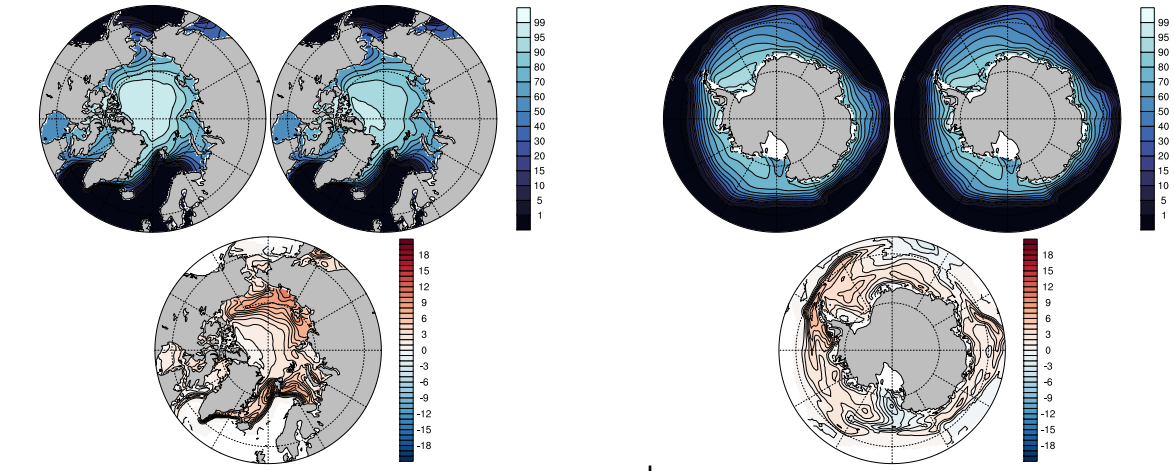

a b

Figure 2. Mean annual sea ice concentration (%) and differences for (a) NH and (b) SH. MUSHY is top left and BL99 is top right. Differences, at bottom center, show MUSHY-BL99 and are only shown where significant at the 5% level.

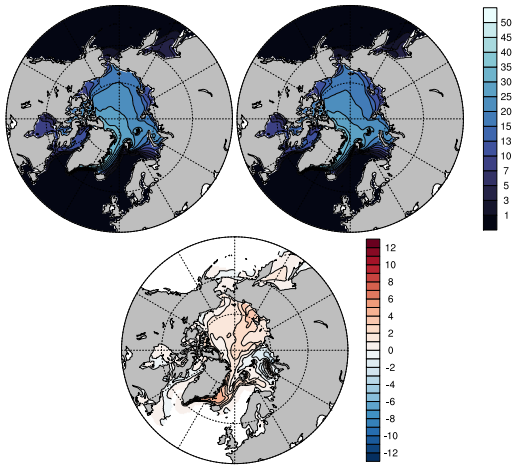

Figure 3. NH mean spring (April-May-June) snow depth (cm) and difference. MUSHY is top left and BL99 is top right. Differences, at bottom center, are MUSHY-BL99 and are only shown where significant at the 5% level.

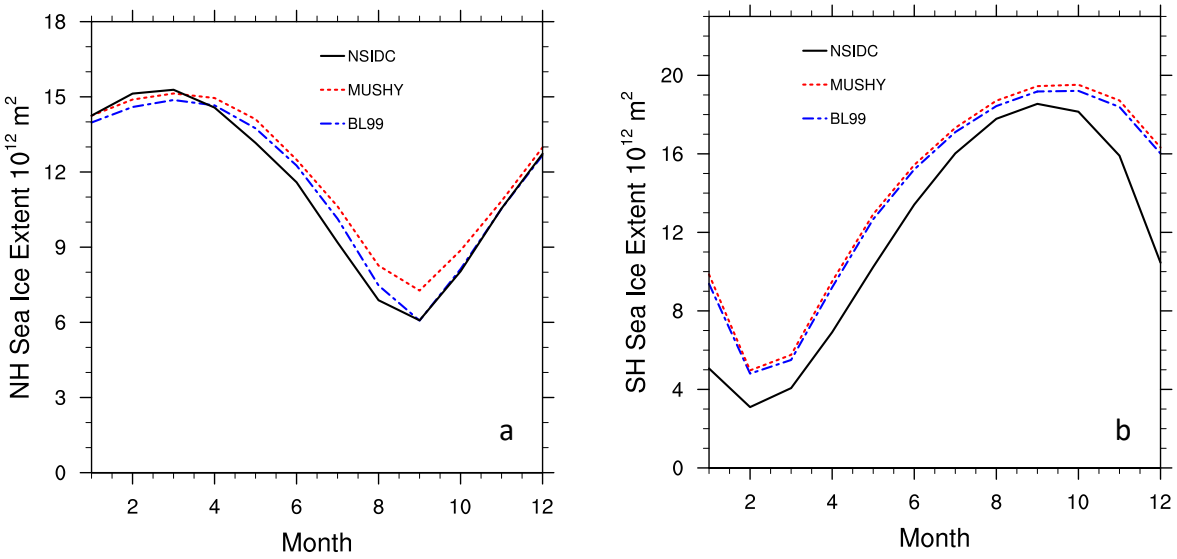

Figure 4. Climatological seasonal cycles of sea ice extent (10^{12} m^2) for (a) NH and (b) SH as compared to the satellite observed NSIDC extent (Fetterer et al. 2017).

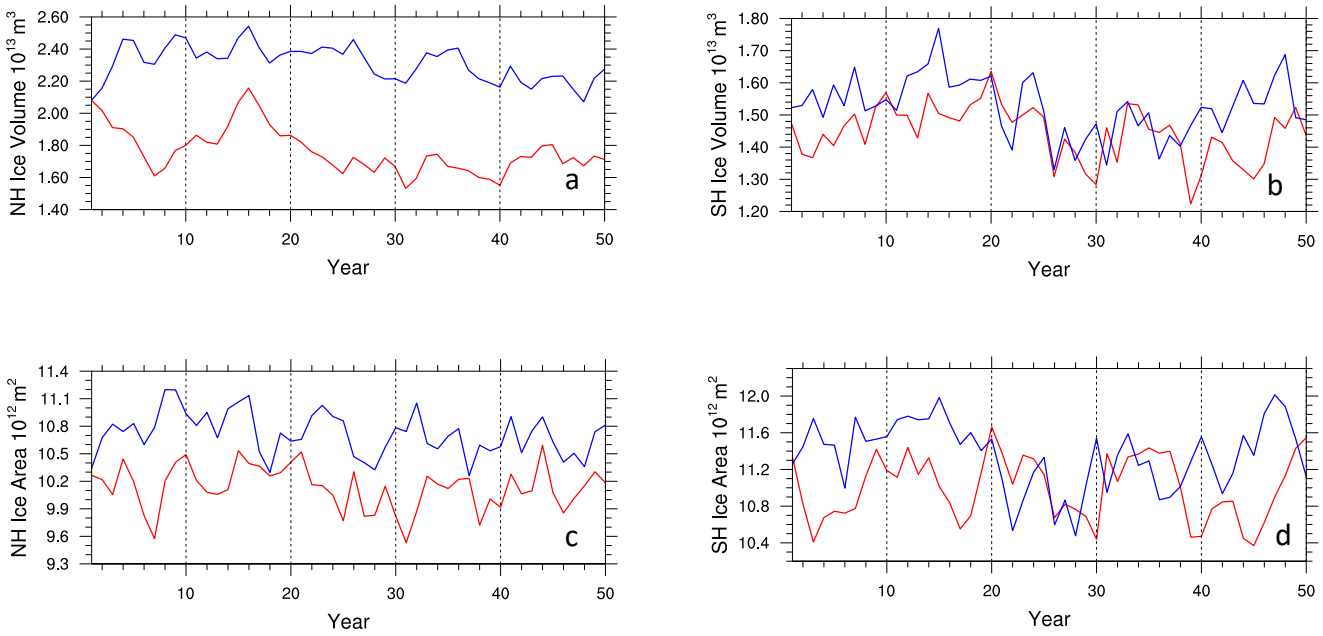

Figure 5. Annual mean sea ice volume (top) and area (bottom) timeseries for MUSHY (red) and BL99 (blue) NH (a and c) and SH (b and d).

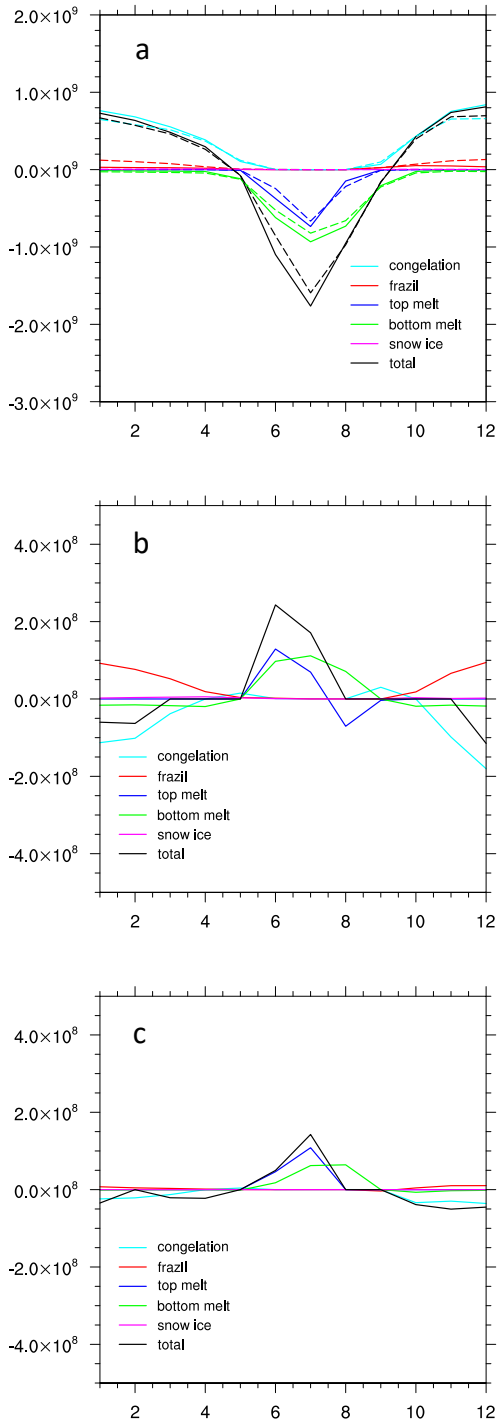

Figure 6. NH (a) annual sea ice mass budget and (b, c) differences in kg/s. In (a) the MUSHY experiment is dashed and the BL99 experiment is solid. In panels b and c, the differences are MUSHY-BL99 for (b) the entire northern hemisphere and (c) the northern hemisphere grid cells with ice concentration greater than 15%. Differences that are not significant at the 95% level are set to 0.

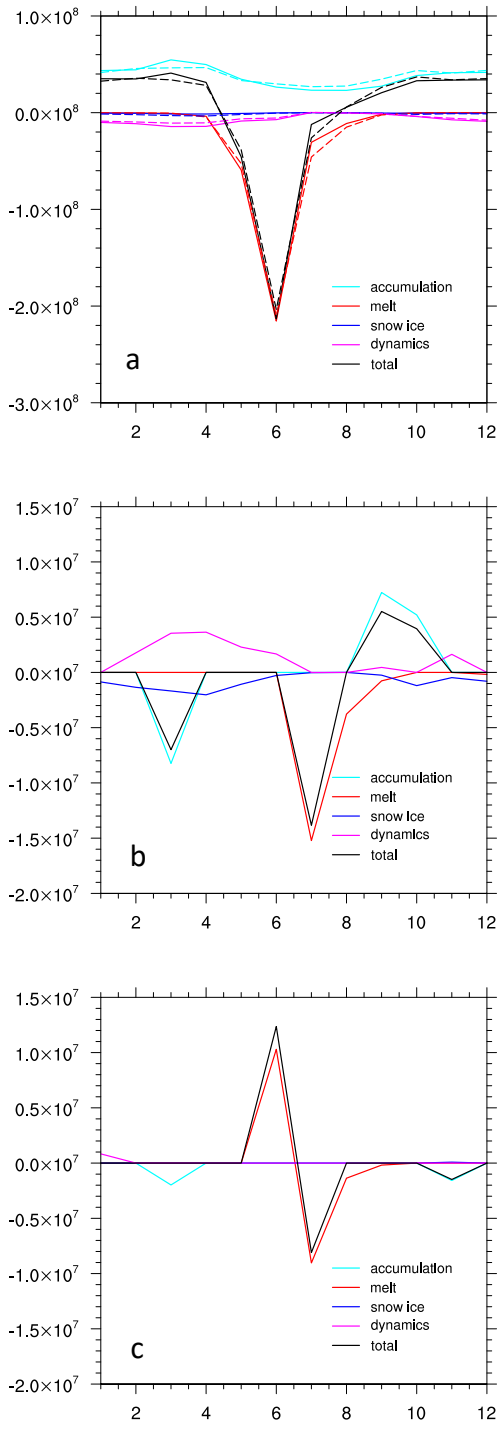

Figure 7: As in Figure 6, for snow.

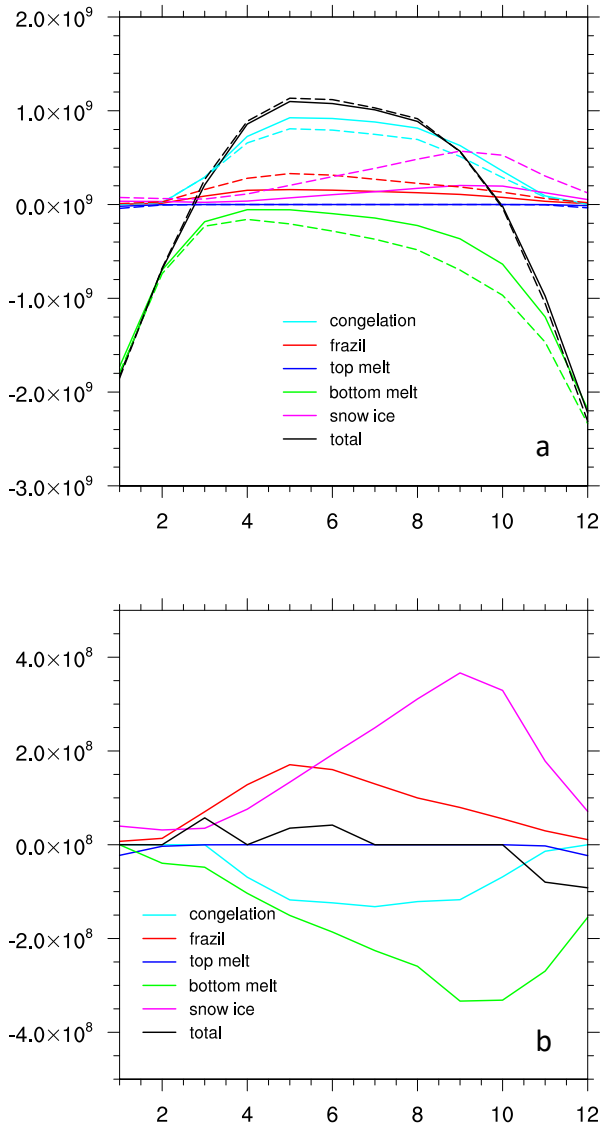

Figure 8. SH (a) annual sea ice mass budget and (b) difference in kg/s. In (a) the MUSHY experiment is dashed and the BL99 experiment is solid. The difference is MUSHY-BL99 and differences that are not significant at the 95% level are set to 0.

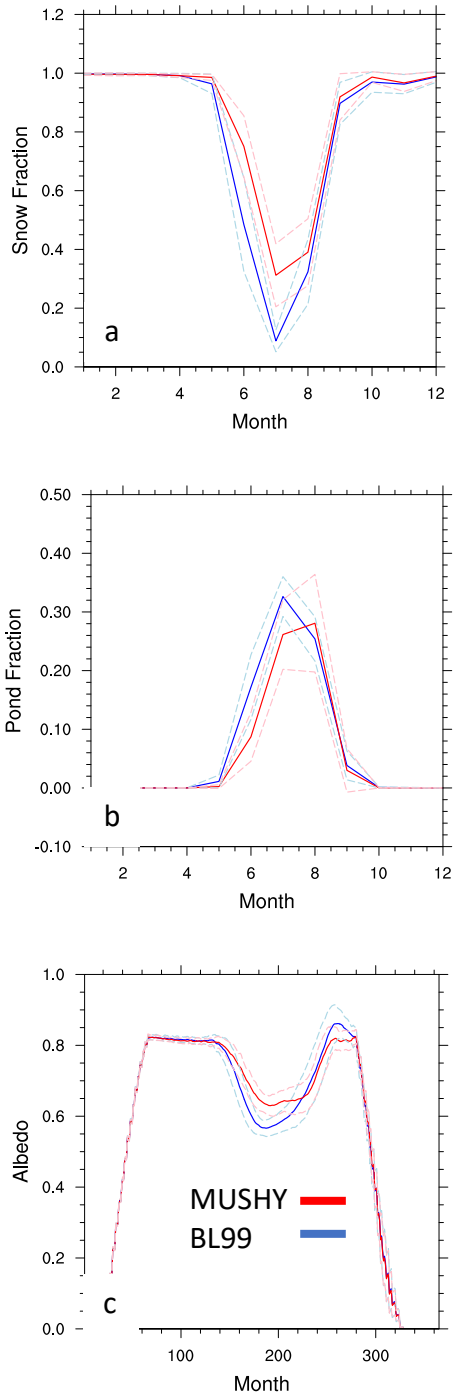

Figure 9. Climatological seasonal cycle of (a) snow fraction, (b) radiatively active melt pond fraction, and (c) surface albedo in a Beaufort Sea region (70-85N, -130 to -180W), with plus and minus one standard deviation (dashed).

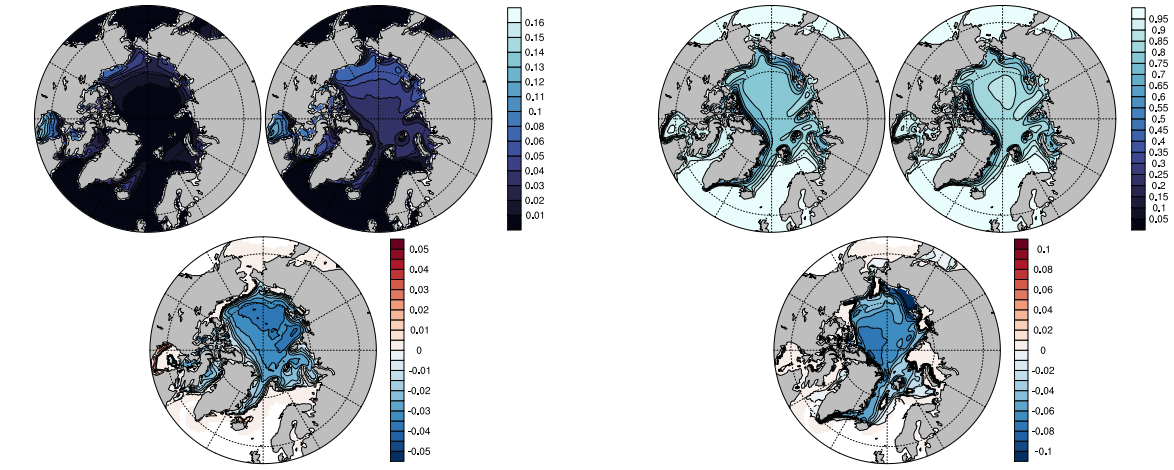

a b

Figure 10. NH April-May-June mean (a) radiatively active pond fraction and (b) level ice fraction. MUSHY is top left and BL99 is top right. Differences, at bottom center, show MUSHY-BL99 and are only shown where significant at the 5% level.

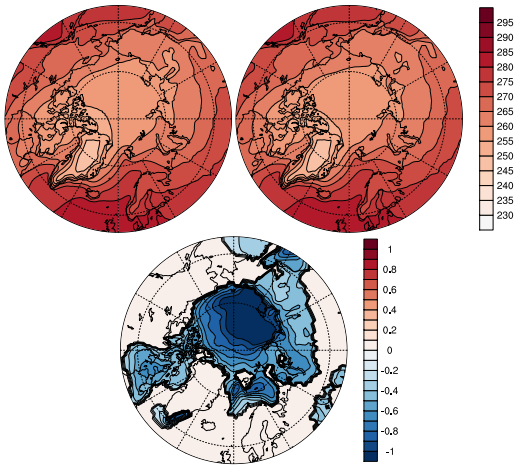

Figure 12. NH annual mean surface air temperature (K) and difference. MUSHY is top left and BL99 is top right. Differences, at bottom center, are MUSHY-BL99 and are are only shown where significant at the 5% level.

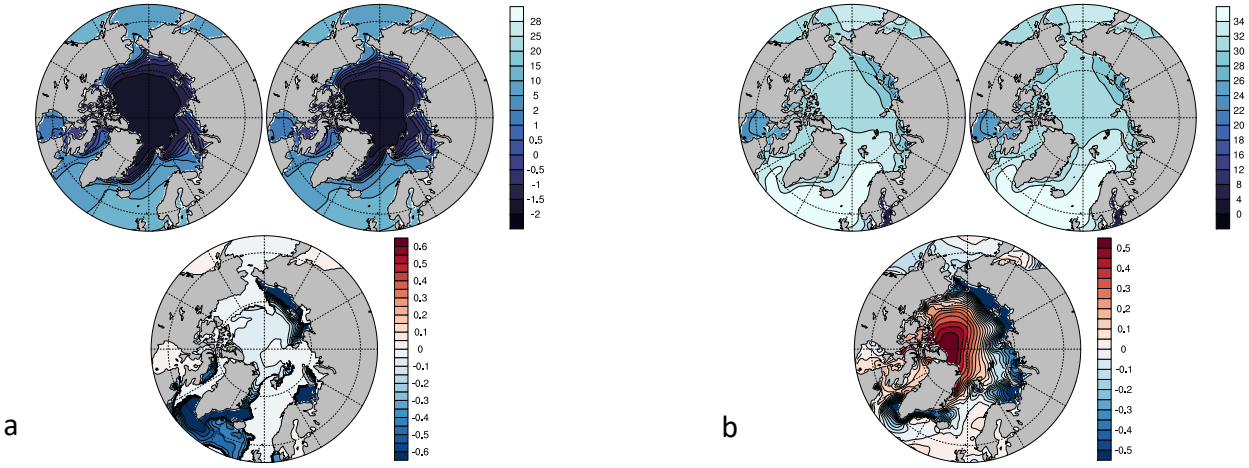

Figure 13. NH July-August-September mean (a) sea surface temperature (°C) and (b) sea surface salinity (psu). MUSHY is top left and BL99 is top right. Differences, at bottom center, show MUSHY-BL99 and are only shown where significant at the 5% level.